

Magnetic anisotropy and magnetization reversal of La_{0.67}Sr_{0.33}MnO₃ thin films on SrTiO₃(110)

Hans Boschker, Jaap Kautz, Evert P. Houwman, Gertjan Koster, Dave H. A. Blank et al.

Citation: *J. Appl. Phys.* **108**, 103906 (2010); doi: 10.1063/1.3506407

View online: <http://dx.doi.org/10.1063/1.3506407>

View Table of Contents: <http://jap.aip.org/resource/1/JAPIAU/v108/i10>

Published by the [American Institute of Physics](#).

Related Articles

Diluted antiferromagnet effect on magnetic and microwave characteristics of exchange-biased multilayered thin films

J. Appl. Phys. **111**, 093919 (2012)

Magnetic vortices in single crystalline Fe-V disks with four folds magnetic anisotropy

Appl. Phys. Lett. **100**, 192406 (2012)

Thickness dependent magnetic properties of amorphous FeTaC films

J. Appl. Phys. **111**, 093915 (2012)

Room-temperature ferromagnetism in epitaxial Mg-doped SnO₂ thin films

Appl. Phys. Lett. **100**, 182405 (2012)

Influence of oxygen vacancies on the electronic structure and magnetic properties of NiFe₂O₄ thin films

J. Appl. Phys. **111**, 093906 (2012)

Additional information on J. Appl. Phys.


Journal Homepage: <http://jap.aip.org/>

Journal Information: http://jap.aip.org/about/about_the_journal

Top downloads: http://jap.aip.org/features/most_downloaded

Information for Authors: <http://jap.aip.org/authors>

ADVERTISEMENT



IBD Optical Film Quality at PVD Rates

Advanced Optical Thin Films

Wide Range of Applications

Superior Throughput and Repeatability

SPECTOR-HT ION BEAM DEPOSITION SYSTEMS

Veeco
Innovation. Performance. Brilliant.

www.veeco.com/spectorht

Magnetic anisotropy and magnetization reversal of $\text{La}_{0.67}\text{Sr}_{0.33}\text{MnO}_3$ thin films on $\text{SrTiO}_3(110)$

Hans Boschker, Jaap Kautz, Evert P. Houwman,^{a)} Gertjan Koster, Dave H. A. Blank, and Guus Rijnders

Faculty of Science and Technology and MESA⁺ Institute for Nanotechnology, University of Twente, 7500 AE Enschede, The Netherlands

(Received 21 July 2010; accepted 25 September 2010; published online 18 November 2010)

The magnetic behavior of $\text{La}_{0.67}\text{Sr}_{0.33}\text{MnO}_3$ (LSMO) films grown on $\text{SrTiO}_3(110)$ substrates was studied. In-plane uniaxial magnetic anisotropy with the easy axis aligned with the [001] lattice direction was observed, together with an out-of-plane component. This is explained by the crystal structure of the films, which shows a tilt of the (001) planes. This tilt creates a long body diagonal which forces the easy axis out-of-plane and results in magnetic domain formation. The domain size is estimated at 500 nm. The switching behavior of the magnetization is well described by a two-phase model which takes both coherent rotation and domain wall motion into account. These results are of importance for the application of LSMO in tunnel magnetoresistance devices, where the (110) orientation is preferred because of the reduction in the dead layer in this direction. © 2010 American Institute of Physics. [doi:10.1063/1.3506407]

I. INTRODUCTION

$\text{La}_{0.67}\text{Sr}_{0.33}\text{MnO}_3$ (LSMO) is a half metal with a Curie temperature of 370 K.¹ Half metals are of great interest for spintronic devices, such as magnetic tunnel junctions (MTJs). In these devices the tunnel current depends on the relative orientation of the two ferromagnetic electrodes. Several examples of LSMO tunnel junctions have been presented in literature,^{2–4} with a maximum obtained tunnel magnetoresistance ratio (TMR) of 4000. However the TMR drops rapidly with temperature and the devices cannot be prepared very reproducibly. The interfacial dead layer of LSMO is thought to be an important cause of the less than ideal behavior.^{5–8} At the interface between LSMO and the barrier material, e.g., SrTiO_3 (STO), the La–Sr ratio surrounding the interfacial Mn ions changes and this results in locally overdoped LSMO.^{9–12} Interface engineering, changing the local cation stoichiometry, has been applied to solve this issue¹³ but with limited success.¹⁴ An alternative approach is to fabricate the tunnel junction on a substrate with pseudocubic (110) orientation.^{15,16} (We will use the pseudocubic notation for LSMO in this paper.) With this orientation the dopants are in the same atomic layer as the Mn ions and no overdoping is expected.

As the TMR depends on the relative orientation of the magnetization in the electrodes, the magnetic anisotropy of the LSMO films, deformed by the strain imposed by the substrate, needs to be studied. STO (110) is a promising substrate for LSMO TMR devices because next to the already discussed (110) orientation, it applies tensile strain to the LSMO. It is known for LSMO thin films that tensile strain results in in-plane magnetization, which reduces magnetic domain formation.^{17–19} The magnetic anisotropy of LSMO on STO (110) was first studied by Suzuki *et al.*²⁰ who found in-plane uniaxial behavior with the easy axis aligned

with the [001] crystal direction. Later studies also found uniaxial anisotropy for films of $\text{La}_{0.67}\text{Ca}_{0.33}\text{MnO}_3$ on STO (110) (Ref. 16) and LSMO on STO (305).²¹

Here, we studied the magnetic behavior of LSMO on STO (110) and we found an overall uniaxial in-plane magnetic anisotropy with an out-of-plane component present as well. This is explained by the observed tilt of the LSMO (001) plane, resulting in an extended body diagonal in the [111] direction. The out-of-plane component results in magnetic domain formation, to reduce the demagnetization energy. Further, we studied the magnetization reversal of the LSMO films, as this is of importance for switching devices such as MTJs. The magnetization reversal is well described by a two-phase model in which both rotation of the magnetization vector in the magnetic domains as well as domain wall motion occurs.

II. EXPERIMENTAL

The as-received STO (110) substrates were cleaned with acetone and ethanol before the anneal treatment. After an annealing step of 1 h at 950 °C in a 1 bar oxygen atmosphere, smooth terraces with straight steppedges, and half unit cell step height (2.7 Å) were observed, using atomic force microscopy (AFM). LSMO thin films were grown on the STO (110) substrates by pulsed laser deposition, from a stoichiometric target in an oxygen background pressure of 0.27 mbar with a laser fluence of 2 J/cm² and at a substrate temperature of 780 °C.⁸ After LSMO deposition, the films were cooled to room temperature in a 1 bar pure oxygen atmosphere.

The crystal structure of the films was determined from x-ray diffraction (XRD) measurements. (Bruker D8 Discoverer equipped with a Vantec-1 array detector) Reciprocal space maps were obtained around the STO (420), (240), (331), and (33 $\bar{1}$) reflections, as shown in Fig. 1. All maps showed an LSMO peak with in-plane momentum transfer

^{a)}Electronic mail: e.p.houwman@utwente.nl.

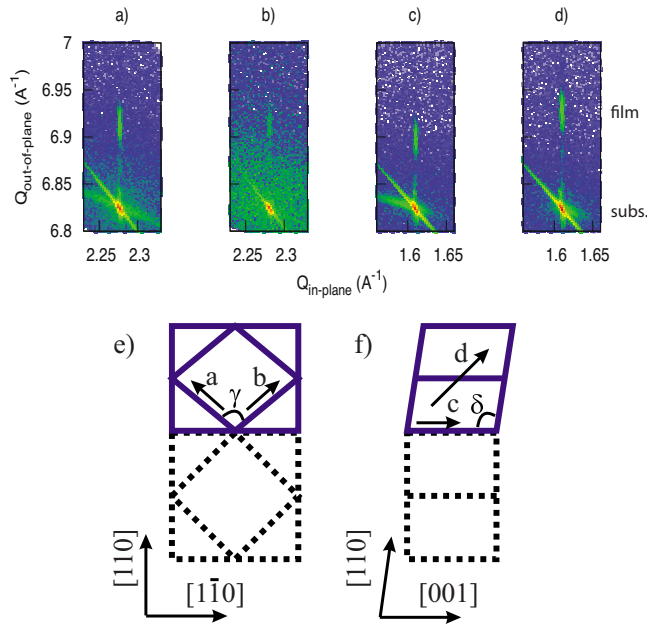


FIG. 1. (Color online) Reciprocal space maps around the (a) (420), (b) (240), (c) (331), and (d) (331 $\bar{1}$) STO reflections of the 22 nm thick sample. All film peaks have in-plane momentum transfer equal to that of the substrate. In (c) and (d) a dissimilar spacing of the (331) and (331 $\bar{1}$) LSMO reflections is clearly observed. This indicates a tilt of the LSMO (001) planes with respect to the [001] lattice vector. A schematic of the crystal structure is shown in (e) and (f) with the view along the [001], respectively, [1 $\bar{1}$ 0] direction. The solid dotted line indicates the STO substrate while the blue line is the LSMO unit cell. The a , b , and c lattice parameters and the long body diagonal d are indicated. The angle δ corresponds to $\angle[(\mathbf{a} + \mathbf{b}), \mathbf{c}]$.

equal to that of the substrate peak, indicating coherent growth and therefore in-plane lattice parameters equal to those of the substrate. Due to the tensile strain the out-of-plane (110) plane spacing of the LSMO is reduced with respect to the bulk value. This results in an angle γ between the \mathbf{a} and \mathbf{b} lattice vectors of 90.8° . We found no significant strain on the $\mathbf{a} = \mathbf{b} = 3.88 \text{ \AA}$ lattice parameters themselves, which are equal to the bulk LSMO values.²² Further, we observed a difference in out-of-plane momentum transfer between the LSMO (331) and (331 $\bar{1}$) reflections. This indicates a tilt of the (001) planes with respect to the plane of the substrate. From the difference we calculate an angle of 90.6° between the LSMO (001) and (110) planes. This results in an angle $\alpha = (\beta =) 90.4^\circ$ between the $\mathbf{b}(\mathbf{a})$ and \mathbf{c} lattice vector. This corresponds well with the angle between the lattice vectors in bulk rhombohedral LSMO (a cube compressed along the [111] direction with $\alpha = \beta = \gamma = 90.35^\circ$). In conclusion LSMO grown on STO (110) has two main deviations from the bulk rhombohedral crystal structure: the \mathbf{c} lattice parameter is elongated to match the lattice parameter of the STO and the angle γ is increased from 90.35° to 90.8° . The lattice parameters and angles are summarized in Table I.

The surface topology of the LSMO films was determined by AFM, showing a smooth surface with roughness at the unit cell step height (2.7 \AA) level. The clear step and terrace structure of the substrate could no longer be observed. The magnetic properties of the samples were characterized with a vibrating sample magnetometer (VSM) (Physical Properties

TABLE I. Lattice parameters of LSMO, grown on STO (110), as determined from XRD measurements. The in-plane lattice parameters are equal to those of the STO (110) surface unit cell. The error in the length is 0.005 \AA and the error in the angle is 0.1° .

LSMO film lattice vectors	Length (\AA)	LSMO angles	Angle (deg)
\mathbf{a}	3.88	α	90.4
\mathbf{b}	3.88	β	90.4
$\mathbf{c} = \mathbf{a}_{\text{STO}}$ (in-plane)	3.905	γ	90.8
$ (\mathbf{a} + \mathbf{b}) $ (out-of-plane)	5.45	$\delta = \angle[(\mathbf{a} + \mathbf{b}), \mathbf{c}]$	90.6
$ (\mathbf{a} - \mathbf{b}) = \sqrt{2}\mathbf{a}_{\text{STO}}$ (in-plane)	5.552	$\angle[(\mathbf{a} - \mathbf{b}), \mathbf{c}]$	90
\mathbf{d} (long body diagonal)	6.82	$\angle[(\mathbf{a} - \mathbf{b}), (\mathbf{a} + \mathbf{b})]$	90
LSMO bulk			
$\mathbf{a} = \mathbf{b} = \mathbf{c}$	3.88	$\alpha = \beta = \gamma$	90.35

Measurement System of Quantum Design and Model 10 VSM of Microsense). The Curie temperature of the samples is 350 K and the low temperature saturation magnetization is $3.7 \mu_B/\text{Mn}$.

III. RESULTS AND DISCUSSION: MAGNETIC PROPERTIES

Angle dependent measurements were performed at room temperature with the field applied in the plane of the film. The in-plane angle of the applied field with the [1 $\bar{1}$ 0] direction was varied to determine the magnetic anisotropy. For all field angles a full magnetization loop was measured and the remanent magnetization, M_r , was obtained from the loop. Figure 2 shows the magnetization loops of a 22 nm sample with the field aligned with the two high symmetry directions. In all figures the linear diamagnetic contribution from the substrate is subtracted. Figure 2(a) shows the magnetization measured parallel to the applied field, M_{par} . Uniaxial behavior is observed; the loop obtained with the applied field parallel to the [001] crystal direction is almost square shaped, indicating that this is the easy axis, while the loop obtained with the field parallel to the [1 $\bar{1}$ 0] direction shows an almost linear dependence of the magnetization on the applied field close to remanence, corresponding to the magnetic hard axis direction. However, the remanent magnetization in the easy direction is only 75% of the saturation value (400 kA/m). This is clearly seen in Fig. 2(b) which shows that the film is saturated only for an applied field larger than about 200 kA/m. Similar behavior for the magnetization loops measured with the field aligned with the [1 $\bar{1}$ 0] and [001] axes was observed for all temperatures down to 10 K, indicating that the easy and hard axis directions do not change with temperature.

The VSM used for this work allows for simultaneous measurement of the two components of the magnetization vector, parallel and perpendicular, M_{perp} , to the field and in the plane of the film. The perpendicular component is presented in Figs. 2(c) and 2(d). When the field is aligned with the easy axis almost no signal is measured, while for the hard axis loop a large magnetization is measured around zero ap-

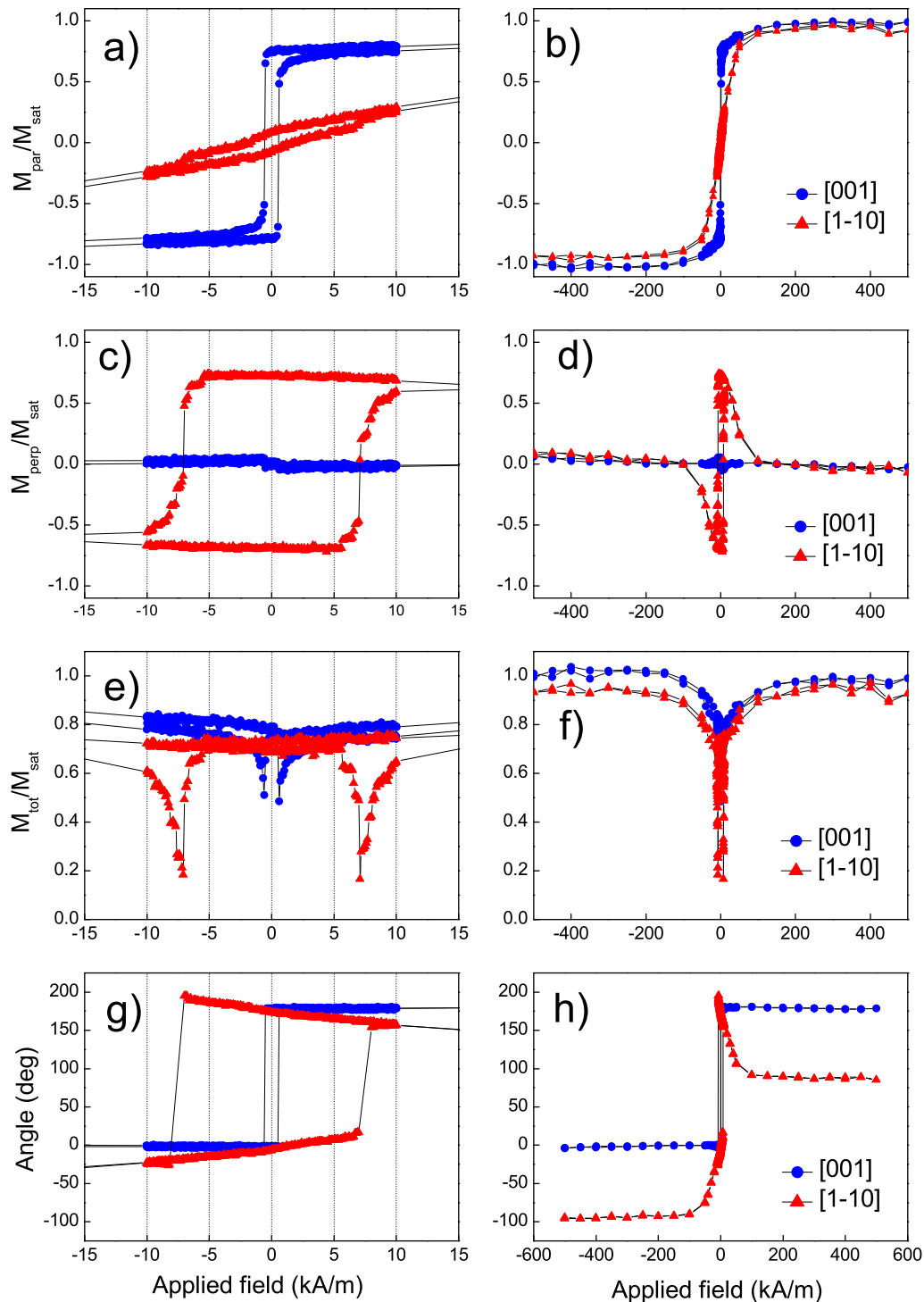


FIG. 2. (Color online) Magnetization loops, circles (triangles) denote measurements with the field aligned with the [001] ($[1\bar{1}0]$) direction. Plotted are (a) and (b) the magnetization parallel to the field (M_{par}), (c) and (d) the magnetization perpendicular to the field and in the plane of the film (M_{perp}), (e) and (f) the total in-plane magnetization ($M_{\text{tot}} = \sqrt{M_{\text{par}}^2 + M_{\text{perp}}^2}$) and (g) and (h) the angle of the magnetization vector with respect to the [001] easy direction (Φ_M). The data has been normalized to the room temperature saturation value (400 kA/m). The left and right columns present identical data, respectively, a close up around remanence and the full loop including saturation. [Note that after the switching of the main domain in the hard axis loop, the angle of the magnetization is not well defined due to the presence of domains which have not yet switched. Therefore no datapoints are presented between 7 and 8 kA/m in figures (g) and (h).]

plied field. This indicates that the magnetization is rotated 90° from the applied field and is aligned with the easy axis, as expected for uniaxial anisotropy. A switch in the magnetization is observed at a field strength of 7 kA/m, at which M_{perp} changes sign. This switching field, H_{sw} , is much larger

than the coercive field of M_{par} shown in Fig. 2(a) and will be discussed later in this paper. Figures 2(e) and 2(f) show the total in-plane magnetization, $M_{\text{tot}} = \sqrt{M_{\text{par}}^2 + M_{\text{perp}}^2}$. Two features deserve attention. The total in-plane magnetization around remanence is only 70% to 80% of the saturation

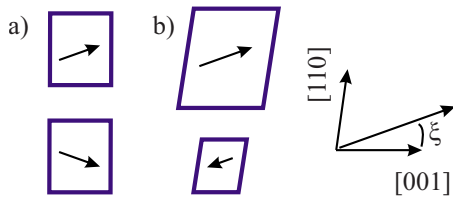


FIG. 3. (Color online) Schematic representation of the magnetization at remanence in the different domains for the case of a partially out-of-plane easy axis. The size of the schematics indicates domain size. (a) Symmetric anisotropy energy with regard to a mirror in the surface plane with easy axes $+\xi$ and $-\xi$ degrees rotated away from the in-plane direction. (b) Anisotropy energy which is not symmetric with respect to a mirror in the surface plane, such as LSMO grown on STO (110). In this case a single easy axis is at $+\xi$.

value. Second, the total in-plane magnetization is reduced at the switching field, especially for the hard axis loop.

The reduction in the remanent magnetization can either be caused by domain formation into domains with opposite in-plane magnetization direction or by a rotation of the magnetization out of the film plane. We assume both mechanisms occur simultaneously. An out-of-plane component to the magnetic anisotropy corresponds well with the observation of an elongated long body diagonal in the [111] direction, Table I. LSMO usually has an easy axis aligned with the maximum tensile strain direction²³ and for LSMO on STO (110) the tilt of the [110] vector in the [001] direction favors a partially out-of-plane easy axis. An out-of-plane component of the easy axis then results in magnetic domain formation due to the high demagnetization energy of a thin film in the out-of-plane direction. This results in domains with alternating out-of-plane component and equal in-plane component of the remanent magnetization. However, in the case of LSMO on STO (110) the symmetry between the two out-of-plane directions is broken due to the tilt of the [110] vector. Therefore domains with alternating out-of-plane components should also have an alternating in-plane component. This alternating in-plane component further reduces the observed remanence. Note that in order to observe any remanence in this domain structure the domains aligned with the previously saturated directions have to be larger compared to the domains in the opposite direction, see Fig. 3.

Figures 2(g) and 2(h) show the angle of the magnetization vector with the [001] easy direction. The angle of the magnetization in the easy axis loop is either 0° or 180° , thus in this case the in-plane magnetization is parallel to the easy axis for all field values, as expected. For the hard axis loop the magnetization rotates from the angle aligned with the field at saturation ($\pm 90^\circ$ for large $|H|$) to the easy axis angle at remanence (respectively, 0° and 180°). When $|H|$ increases from zero after switching sign for increasing and decreasing field the (in-plane) magnetization angle increases further to about 20° and 200° , respectively at the switching field, $H_s = 7$ kA/m. At the switching field the magnetization suddenly switches almost 180° and for high field strength the magnetization rotates toward the field direction again.

In Fig. 4(a) we plotted the dependence of the remanent magnetization on the in-plane field angle. The angular dependence is typical for predominantly uniaxial anisotropy of

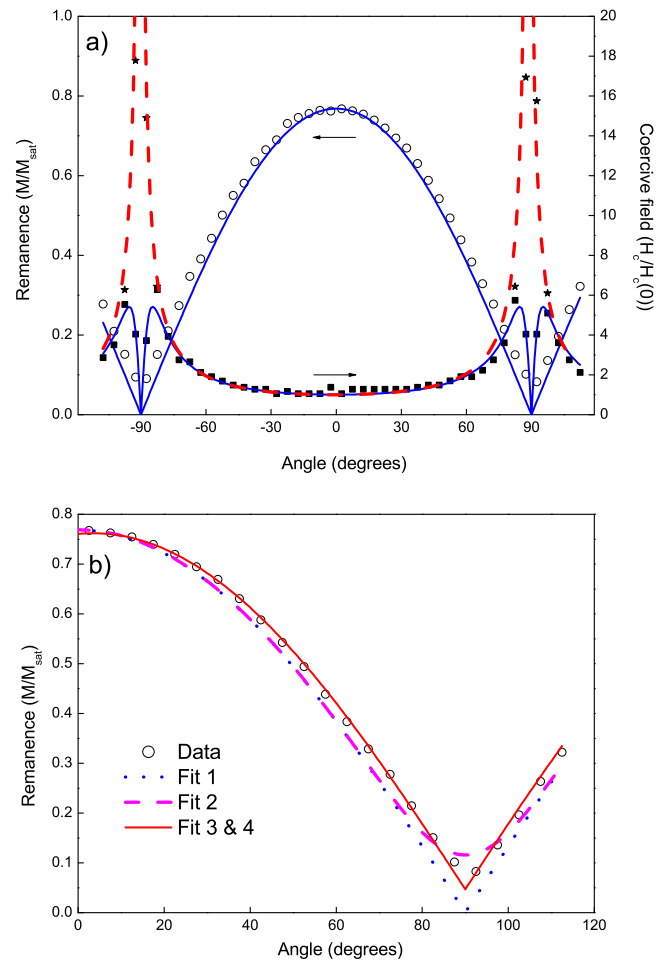


FIG. 4. (Color online) (a) Angular dependence of the remanent magnetization (open circles), coercivity (closed squares), and switching field (closed stars). The data has been normalized to the room temperature saturation values [$M_{\text{sat}}=400$ kA/m and $H_c(0)=0.47$ kA/m]. The fits are based on the models described in the text. (b) Angular dependence of the remanence fitted with four different models: (1) single easy axis (dotted line), (2) Gaussian distribution of easy axes (dashed line), (3) biaxial anisotropy contribution (solid line), and (4) magnetization aligned partially with the hard axis direction (solid line).

the sample, where the magnetization, which is aligned with the easy axis at zero applied field, is projected onto the direction of measurement:

$$M_{\text{rem}}(\theta) = M_0 \cos(\theta), \quad (1)$$

in which M_{rem} is the remanent magnetization, θ is the angle between the applied field and the easy axis direction, and M_0 is the remanence in the easy direction. This relation is plotted with the solid blue line in the figure. There is some deviation from ideal behavior, especially pronounced in the hard direction, where the remanence is not equal to zero.

Four fits to the remanence data are plotted in Fig. 4(b): ideal uniaxial behavior, uniaxial behavior with a spread in easy axis directions, a combination of uniaxial and biaxial behavior, and uniaxial behavior with a magnetization contribution aligned with the hard axis. For all fits the value of the remanence at 0° was fixed. The dotted blue line is the ideal uniaxial behavior, Eq. (1), also shown in Fig. 4(a). The dashed magenta line, fit 2, is the fit based on the model with a Gaussian spread in easy axes distribution, e.g., due to strain

relaxation into different grains of the film. In this case, the best fit was obtained for a distribution centered around 0° and with a standard deviation of 11° . It does not fit the data well, from 10° to 70° the model predicts a smaller remanence while around the hard axis the model predicts a smooth, rounded angular dependence which is also not observed. The other two fits, 3 and 4, describe the data very well. Fit 3 is based on the model which includes a biaxial contribution to the anisotropy. This results in a system with two easy axes, located symmetrically around the uniaxial easy direction.²⁴ From the fit easy axes at 3.5° and -3.5° are obtained. Fit 4 assumes that a part of the magnetization is aligned with the hard axis at zero field. This part is 4.5% of the easy axis magnetization for the fit presented in the figure. Although fit 3 and 4 result in identical remanence curves, the physical interpretation is different. If the sample would have two different easy axes, the magnetization curves should show double switching. At the first switch the magnetization angle should change by 7° and then only at the second switch should the magnetization be reversed. The switch of 7° is clearly not observed in Fig. 2(g) which shows a smooth rotation of the magnetization. Therefore, we conclude that the sample has a single easy axis at 0° and fit 4 is the right interpretation of the data. Previously we concluded that the magnetization at remanence consists of different domains. We therefore attribute the 4.5% magnetization aligned in the hard axis direction to the magnetic signal contained in the domain walls. This implies Bloch domain walls.

Now that the amount of magnetization in the domain walls is known, we can calculate the average domain size using the domain wall thickness. The latter can be estimated with²⁵

$$\delta = \pi \sqrt{\frac{JS^2}{K_u a}}, \quad (2)$$

in which δ is the domain wall thickness, J is the exchange integral, $S=1.85$ is the spin of an Mn ion, $K_u=7$ kJ/m³ is the uniaxial anisotropy energy, and a is the interatomic distance between the Mn ions. K_u was determined from the hard axis magnetization loop. The exchange integral J is equal to²⁶

$$J = \frac{3k_B T_C}{2zS(S+1)} = 2.4 \times 10^{-22} \text{ J}, \quad (3)$$

in which k_B is Boltzman's constant, T_C is the Curie temperature, and $z=6$ is the number of nearest neighbors. Using these values we estimate a domain wall thickness of 55 nm. With two times 4.5% of the magnetization present in the domain walls, it follows that the average domain size is 500 nm.

Figure 4(a) also shows the angular dependence of the coercive field. An M-shaped curve is observed with the maximum coercive field at an angle of 5° – 10° from the hard axis. Similar curves were observed for LSMO grown on NdGaO₃ and indicate magnetization reversal by a combination of domain wall motion and magnetization rotation.²⁷ The curve can be described with the relation²⁸

$$H_c(\theta) = H_c(0) \frac{(N_x + N_N) \cos \theta}{N_z \sin^2 \theta + (N_x + N_N) \cos^2 \theta}, \quad (4)$$

in which H_c is the coercive field, N_z and N_x are the demagnetizing factors in the z-axis direction (corresponding to the in-plane easy axis direction of the thin films considered here) and x-axis direction, respectively. Both axes are in the plane of the magnetic field and of the magnetization rotation. $N_N = H_A/M_s$ is a formal parameter which describes an effective demagnetization factor other than shape anisotropy. H_A is the anisotropy field and M_s is the saturation magnetization. The ratio $y = (N_x + N_N)/N_z = 116$ and $H_c(0) = 0.47$ kA/m are used as fit parameters to obtain the fit in the figure. The two-phase model describes the angular dependence of coercivity well and is in agreement with the magnetization loops shown in Fig. 2. The reduction in the total magnetization during the switching, Fig. 2(e), is naturally explained by the presence of magnetic domains with opposite magnetization directions. In Fig. 4(a) we also plotted the angular dependence of the switching field, H_{sw} , which deviates from the coercive field close to the hard axes. Where the coercive field approaches zero at the hard axes in the two-phase model due to the rotation of magnetization in the domains, the switching field is largest for values close to the hard axes. The switching field is fitted well with the Kondorsky²⁹ relation for domain wall motion $H_{sw} = H_{sw}(0)/\cos \theta$.

IV. CONCLUSION

In conclusion, the magnetic behavior of LSMO films grown on STO (110) substrates was studied. Next to the earlier observed in-plane uniaxial magnetic anisotropy with the easy axis aligned with the [001] lattice direction, we found evidence for an out-of-plane component to the magnetic anisotropy. This can be explained by the crystal structure of the films, that shows a tilt of the (001) planes. This tilt creates a long body diagonal which forces the easy axis out-of-plane and results in magnetic domain formation with an estimated domain size of 500 nm. We found that the switching behavior of the magnetization is well described by a two-phase model which takes both coherent rotation and domain wall motion into account. These results are of importance for the application of LSMO in TMR devices, where the (110) orientation is preferred because of the reduction in the dead layer in this direction. Our results indicate that the device area should be smaller than 500×500 nm² for optimum TMR performance as then the tunneling from a single magnetic domain is measured.

ACKNOWLEDGMENTS

This research was financially supported by the Dutch Science Foundation, by NanoNed, a nanotechnology program of the Dutch Ministry of Economic Affairs, and by the NanOxide program of the European Science Foundation.

¹J. Park, E. Vescovo, H. Kim, C. Kwon, R. Ramesh, and T. Venkatesan, *Nature (London)* **392**, 794 (1998).

²J. O'Donnell, A. E. Andrus, S. Oh, E. V. Colla, and J. N. Eckstein, *Appl. Phys. Lett.* **76**, 1914 (2000).

³M. Bowen, M. Bibes, A. Barthelemy, J. Contour, A. Anane, Y. Lemaitre,

- and A. Fert, *Appl. Phys. Lett.* **82**, 233 (2003).
- ⁴Y. Ogimoto, M. Izumi, A. Sawa, T. Manako, H. Sato, H. Akoh, M. Kawasaki, and Y. Tokura, *Jpn. J. Appl. Phys., Part 2* **42**, L369 (2003).
- ⁵J. Sun, D. Abraham, R. Rao, and C. Eom, *Appl. Phys. Lett.* **74**, 3017 (1999).
- ⁶R. Borges, W. Guichard, J. Lunney, J. Coey, and F. Ott, *J. Appl. Phys.* **89**, 3868 (2001).
- ⁷M. Angeloni, G. Balestrino, N. Boggio, P. Medaglia, P. Orgiani, and A. Tebano, *J. Appl. Phys.* **96**, 6387 (2004).
- ⁸M. Huijben, L. W. Martin, Y. H. Chu, M. B. Holcomb, P. Yu, G. Rijnders, D. H. A. Blank, and R. Ramesh, *Phys. Rev. B* **78**, 094413 (2008).
- ⁹H. Kumigashira, A. Chikamatsu, R. Hashimoto, M. Oshima, T. Ohnishi, M. Lippmaa, H. Wadati, A. Fujimori, K. Ono, M. Kawasaki, and H. Koinuma, *Appl. Phys. Lett.* **88**, 192504 (2006).
- ¹⁰H. Kumigashira, R. Hashimoto, A. Chikamatsu, M. Oshima, T. Ohnishi, M. Lippmaa, H. Wadati, A. Fujimori, K. Ono, M. Kawasaki, and H. Koinuma, *J. Appl. Phys.* **99**, 08S903 (2006).
- ¹¹J. W. Freeland, J. J. Kavich, K. E. Gray, L. Ozyuzer, H. Zheng, J. F. Mitchell, M. P. Warusawithana, P. Ryan, X. Zhai, R. H. Kodama, and J. N. Eckstein, *J. Phys.: Condens. Matter* **19**, 315210 (2007).
- ¹²J. J. Kavich, M. P. Warusawithana, J. W. Freeland, P. Ryan, X. Zhai, R. H. Kodama, and J. N. Eckstein, *Phys. Rev. B* **76**, 014410 (2007).
- ¹³H. Yamada, Y. Ogawa, Y. Ishii, H. Sato, M. Kawasaki, H. Akoh, and Y. Tokura, *Science* **305**, 646 (2004).
- ¹⁴Y. Ishii, H. Yamada, H. Sato, H. Akoh, Y. Ogawa, M. Kawasaki, and Y. Tokura, *Appl. Phys. Lett.* **89**, 042509 (2006).
- ¹⁵Y. Mukunoki, N. Nakagawa, T. Susaki, and H. Hwang, *Appl. Phys. Lett.* **86**, 171908 (2005).
- ¹⁶I. C. Infante, F. Sanchez, J. Fontcuberta, S. Fusil, K. Bouzehouane, G. Herranz, A. Barthelemy, S. Estrade, J. Arbiol, F. Peiro, R. J. O. Mossaneck, M. Abbate, and M. Wojcik, *J. Appl. Phys.* **101**, 093902 (2007).
- ¹⁷C. Kwon, M. Robson, K. Kim, J. Gu, S. Lofland, S. Bhagat, Z. Trajanovic, M. Rajeswari, T. Venkatesan, A. Kratz, R. Gomez, and R. Ramesh, *J. Magn. Magn. Mater.* **172**, 229 (1997).
- ¹⁸R. Desfeux, S. Bailleul, A. Da Costa, W. Prellier, and A. Haghiri-Gosnet, *Appl. Phys. Lett.* **78**, 3681 (2001).
- ¹⁹J. Dho, Y. Kim, Y. Hwang, J. Kim, and N. Hur, *Appl. Phys. Lett.* **82**, 1434 (2003).
- ²⁰Y. Suzuki, H. Hwang, S. Cheong, and R. vanDover, *Appl. Phys. Lett.* **71**, 140 (1997).
- ²¹M. van Zalk, M. Veldhorst, A. Brinkman, J. Aarts, and H. Hilgenkamp, *Phys. Rev. B* **79**, 134509 (2009).
- ²²A. Hammouche, E. Siebert, and A. Hammou, *Mater. Res. Bull.* **24**, 367 (1989).
- ²³H. Boschker, M. Mathews, E. P. Houwman, H. Nishikawa, A. Vailionis, G. Koster, G. Rijnders, and D. H. A. Blank, *Phys. Rev. B* **79**, 214425 (2009).
- ²⁴H. Boschker, M. Mathews, P. Brinks, E. P. Houwman, A. Vailionis, G. Koster, G. Rijnders, and D. H. A. Blank, arXiv:1009.0815 (unpublished).
- ²⁵S. Chikazumi, *Physics of Ferromagnetism*, 2nd ed. (Clarendon, Oxford, 1997).
- ²⁶C. Kittel, *Introduction to Solid State Physics*, 5th ed. (Wiley, New York, 1976).
- ²⁷M. Mathews, E. P. Houwman, H. Boschker, G. Rijnders, and D. H. A. Blank, *J. Appl. Phys.* **107**, 013904 (2010).
- ²⁸N. Suponev, R. Grechishkin, M. Lyakhova, and Y. Pushkar, *J. Magn. Magn. Mater.* **157–158**, 376 (1996).
- ²⁹E. Kondorsky, *J. Phys. (USSR)* **2**, 161 (1940).